www.czasopisma.pan.pl PAN POLSKA AKADEMIA NAUK www.journals.pan.pl

PAN ARCHIVES OF ACOUSTICS
Vol. 42, No. 4, pp. 619–629 (2017)

DOI: 10.1515/aoa-2017-0066

A Fast Method of Feature Extraction for Lowering Vehicle Pass-By Noise Based on Nonnegative Tucker3 Decomposition

Haijun WANG, Guo CHENG, Guoyong DENG, Xueping LI, Honggeng LI, Yuanyi HUANG

NVH Research Department, SAIC-GM-Wuling Automobile CO., LTD
18 Hexi Road, Liuzhou, Guangxi, China;
e-mail: whjun69@sina.com, {Guo.Cheng, Guoyong.Deng, Xueping.Li, Honggeng.Li, Yuanyi.Huang}@sgmw.com.cn

(*received December 15, 2016; accepted May 9, 2017*)

Usually, the judgement of one type fault of vehicle pass-by noise is difficult for engineers, especially when some significant features are disturbed by other interference noise, such as the squealing noise is almost simultaneous with the whistle in the exhaust system. In order to cope with this problem, a new method, with the antinoise ability of the algorithm on the condition by which the features are entangled, is developed to extract clear features for the fault analysis. In the proposed method, the nonnegative Tucker3 decomposition (NTD) with fast updating algorithm, signed as NTD_FUP, can find out the natural frequency of the parts/components from the exhaust system. Not only does the NTD_FUP extract clear features from the confused noise, but also it is superior to the traditional methods in practice. Then, an aluminium-foil alloy material, which is used for the heat shield for its lower noise radiation, replaces the aluminium alloy alone. Extensive experiments show that the sound pressure level of the vehicle pass-by noise is reduced 0.9 dB(A) by the improved heat shield, which is also considered as a more lightweight design for the exhaust system of an automobile.

Keywords: vehicle pass-by noise; NTD; feature extraction; sound pressure level.

1. Introduction

The problem of road traffic noise in the living environment has attracted a lot of attention due to concerns for human health and life quality. One of the essential reasons discovered in a comprehensive investigation is vehicle exterior noise in the pass-by driving manoeuvre (Park, Kim, 2001), which is an awful burden to people resulting in annoyance, sleep disturbance, or cardiovascular disease (Okokon *et al.*, 2015). Governments in European countries have already revised the standard ISO 362, which is stringent for the environmental protection, regulation of emissions control of vehicle pass-by noise (Braun *et al.*, 2013). Sequentially, the sound pressure level (SPL) is well reduced from 84 dB(A) to 76 dB(A) for K-cars in China (Beijing Labour Protection Research, 2002, p. 2). Presently, a stricter version as 74 dB(A) for noise control in the next stage is being considered. The reduction of SPL, in a sense, becomes a very urgent task due to the regulation requirement (Nilsson, 2007). Therefore, how to develop an efficient way to extract pure features is one of the most crucial issues for fault interpretation. We note that nonnegative Tucker3 decomposition (NTD) (Andersson, Bro, 1998), which is enforced on nonnegative constraints (Kim *et al.*, 2007), may be an excellent method to extract features from the vehicle pass-by noise.

NTD involves in feature extraction in many field works ranging from blind source separation (Cichocki *et al.*, 2009), images (Wang *et al.*, 2011), systems biology (Xu, Yin, 2013), and others (Kopriva, Cichocki, 2010). The advantage of NTD is in less computation storage needed as compared with other traditional methods, such as nonnegative matrix factorisation (NMF) and nonnegative tensor factorisation (NTF), which also reflect the frequency by the basic images of features extracted (Cichocki, Amari, 2010). Actually, NTD, known as well as a tensor tool generalising the standard matrix to data arrays of order higher than two (Lim, Comon, 2010), has been developed into a general form of NMF/NTF. Besides, the updating algorithm of factors is used to overcome the problem of data overfitting in the iteration, namely robustness (Wang *et al.*, 2013a). More properties about NTD can be found in (Andersson, Bro, 1998).

The SPL of vehicle pass-by noise is mostly proportional to the speed of the engine, in the case of wide open throttle (WOT) when the accelerator pedal is fully depressed. To objectively evaluate the SPL, vehicle pass-by noise both at the 2-nd gear (2G) and the 3-rd gear (3G) is measured by WOT. Then the SPL is checked with A-weighting way whether the noise meets the regulation, which is also used to evaluate the NVH (Noise, Vibration and Harshness) level of an automobile (Nilsson, 2007, cited by Wang *et al.*, 2016). Mostly, vibration resonance, noise radiation, or both statuses may occur when the vibration and noise interfere with each other, especially with two or more near natural frequencies, for example, the possibility between the heat shield and the exhaust pipe (Davies, Harrison, 1997).

In our case, the higher SPL is caused by the property of the stiffness and damping of the material (Romanowicz, 2014). In order to analyse the high noise, conjugating with the feature bispectum of the parts/components in the exhaust system, we find that the noise radiation roots are frequently in the surface of the heat shield. The aluminum-foil alloy material, used for the heat shield, replaces the current aluminum alloy alone. New heat shield damping and stiffness, also considered as the main contribution to the SPL, are improved by the structural design and material selection. Lastly, the NTD method is comprehensively verified by the spectral analysis due to the feature extraction and fault interpretation in the SPL problem solution.

2. Sub-tensor decompositon for the vehicle pass-by noise

As to vehicle pass-by noise the response signal approximates to a sinusoid wave at the centre frequency of a normal-mode filtering method (Mongia, Bhartia, 1994) The equation can be written as

$$F(t) = at^{N-1}\exp(-2\pi bt)\cos(2\pi f_c + \varphi) \qquad (t \geq 0, N \geq 1), \quad (1)$$

where a is the amplitude normalised for the peak magnitude N is the data order, b is the value that determines the bandwidth of the wave signal f_c is the centre frequency φ is the phase of the noise signal. Patterson and Gillette (1977) give the relationship between b and f_c according to the psychological characteristics then, the bandwidth $b$is represented as

$$b(f_c) = 1.019 \cdot 24.7(1 + 4.37 f_c/1000). \quad (2)$$

Generally, the bispectrum exists as a matrix or vector after the transformation from time domain into frequency domain. However, most features are in a chaotic distribution at the initial state. Therefore all the signals need to be preprocessed as a tensor or vector for well-ordered computation. The relationship between a tensor and mode matrices directing to time is expressed in Fig. 1.

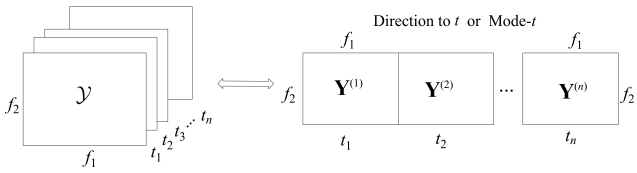

Fig. 1. Relationship between the tensor and mode matrices.

The conversion, as well known as matricisation, is the rearrangement of the slices of a tensor into a matrix or vector, marked as $vec(\cdot)$. For a given tensor $\mathcal{Y} \in \mathbb{R}^{I_1 \times \cdots \times I_N}$, there exists a subset $n := \{1, 2, \cdots, N\}$ of dimension indices, the relationship is,

$$\begin{aligned} &\mathcal{Y}^{(n)} \in \mathbb{R}^{I_n \times I_s}, \\ &\mathbb{I}_n := \{I_1, I_2, \cdots, I_N\}, \\ &\mathbb{I}_s := \prod_{s \neq n} I_s. \end{aligned} \quad (3)$$

Thus, the process of tensor decomposition will be kept on when the higher order array is completely rearranged for the feature extraction.

2.1. Physical model of Tucker3 decomposition to subtensors

Assume the vehicle pass-by noise is a real time-domain signal, which is composed by a set of third-order subtensors $\{\mathcal{Y}_k | k = (i_{k,1}, i_{k,2}, i_{k,3})\} :\in \mathcal{Y} \in \mathbb{R}^{I_1 \times I_2 \times I_3}$ $(i_{k,1} \in I_1,\ i_{k,2} \in I_2,\ i_{k,3} \in I_3)$, where k is the subtensor index. By decomposing it into a core tensor $\mathcal{G}_k$ and three mode matrices $\{\mathbf{A}_k^{(n)}\} : (n \leq 3)$ with Tucker3 decomposition the algorithm can be written as

$$\begin{aligned} &\mathcal{Y}_k = \widehat{\mathcal{Y}}^{(k)} + \mathbf{E}^{(k)} = \mathcal{G}_k \times_1 \mathbf{A}_k^{(1)} \times_2 \mathbf{A}_k^{(2)} \times_3 \mathbf{A}_k^{(3)} + \mathbf{E}_k \\ &\text{or} \qquad \mathcal{Y}_k \approx \mathbf{A}_k^{(n)} \mathbf{G}_k^{(n)} \mathbf{A}_k^{\otimes -n} \\ &\text{s.t.} \qquad \mathbf{A}_k^{\otimes} = \mathbf{A}_k^{(1)} \otimes \mathbf{A}_k^{(2)} \otimes \mathbf{A}_k^{(3)}, \end{aligned} \quad (4)$$

where $\widehat{\mathcal{Y}}_k$ approximates to its real-valued $\mathcal{Y}_k$, symbol $\times_n$ denotes the mode product between the core tensor and the mode matrices $\otimes$ denotes the Kronecker product $\mathbf{A}_k^{\otimes -n}$ is the Kronecker product of all mode matrices except $\mathbf{A}_k^{(n)}$, $\mathbf{G}_k^{(n)}$ is an unfold form of core tensor $\mathcal{G}_k \in \mathbb{R}^{J_1 \times J_2 \times J_3}$ $(J_n \leq I_n,\ n = 1, 2, 3)$ (Kopriva, Cichocki, 2010) directing to n. The eigenvalues in the core tensor are arranged in the order of feature weightiness, which leaves the core tensor if the eigenvalues are less than 10^{-3}. The core tensor and the mode matrices make a product when J_n is fixed. For observation, Tucker3 decompositon based on Eq. (4) is illustrated in Fig. 2.

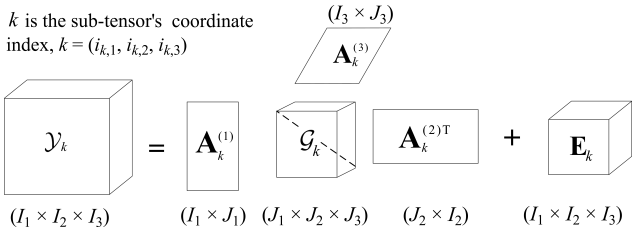

Fig. 2. Model of Tucker3 decomposition to a subtensor.

All factors, including the core tensor $\mathcal{G}_k$ and mode matrices $\mathbf{A}_k$, reconstruct the basis images of features after a tensor is completely decomposed. Herein, the physical model provides local bispectrum features for fault interpretation.

2.2. Algorithmic simplification for Tucker3 decomposition

The factors involving in $\mathbf{A}_k$ and $\mathcal{G}_k$ can be calculated by the way of alternating least square (ALS) (Hemmateenejad *et al.*, 2008), which uses the way of parallel computation for less computer storage. Besides, part calculation is implemented on Matlab (2012b) by the tensor toolbox (Bader, Kolda, 2006). The cost function based on the Frobenius norm for ALS is written as:

$$D_k^{(n)} = \frac{1}{2}\left\|\mathrm{vec}(\mathcal{Y}_k)^{(n)} - \mathbf{A}_k^{(n)}\mathbf{G}_k^{(n)}\{\mathbf{A}_k^{\otimes -n}\}^{\mathrm{T}}\right\|_{\mathrm{F}}^2, \quad k = (i_{k,1}, i_{k,2}, i_{k,3}), \tag{5}$$

s.t.

$$\mathbf{A}_k^{\otimes -n} = \mathbf{A}_k^{(n+1)} \otimes \cdots \otimes \mathbf{A}_k^{(N)} \otimes \mathbf{A}_k^{(1)} \otimes \mathbf{A}_k^{(2)} \otimes \cdots \otimes \mathbf{A}_k^{(n-1)},$$

where $\|\cdot\|_{\mathrm{F}}$ denotes the Frobenius norm. Operator $\mathrm{vec}(\cdot)$ is an unfold form of the subtensor $\mathcal{Y}_k$. Now let us take partial differentiation on $D_k^{(n)}$ as to $\mathbf{A}_k^{(n)}$ in Eq. (5), that is,

$$\min \ \nabla_{\mathbf{A}_k^{(n)}} D_k^{(n)} = \left(\mathbf{Y}_k^{(n)} - \mathbf{A}_k^{(n)}\mathbf{G}_k^{(n)}\{\mathbf{A}_k^{\otimes -n}\}^{\mathrm{T}}\right) \cdot \{\mathbf{A}_k^{\otimes -n}\}\mathbf{G}_k^{(n)\mathrm{T}}, \tag{6}$$

where $\mathbf{Y}_k^{(n)}$ is an unfold form of $\mathcal{Y}_k$ directing to n. The right part of Eq. (6) approximates to zero, while the gradient convergence returns to a minimum value. Also Eq. (6) derives the multiplicative iteration for NTD in progress. We transpose all the polynomials above, then the mode-n matrix $\mathbf{A}_k^{(n)}$ can be expressed as

$$\mathbf{A}_k^{(n)} \leftarrow \frac{\mathbf{Y}_k^{(n)}\mathbf{A}_k^{\otimes -n}}{\mathbf{G}_k^{(n)}\{\mathbf{A}_k^{\otimes -n}\}^{\mathrm{T}}\{\mathbf{A}_k^{\otimes -n}\}} = \frac{\mathbf{Y}_k^{(n)}\mathbf{A}_k^{\otimes -n}}{a^*}, \tag{7}$$

where

$$a^* = \mathbf{G}_k^{(n)}(\mathbf{A}_k^{(n+1)\mathrm{T}}\mathbf{A}_k^{(n+1)} \otimes \cdots \otimes \mathbf{A}_k^{(N)\mathrm{T}}\mathbf{A}_k^{(N)} \otimes \mathbf{A}_k^{(1)\mathrm{T}}\mathbf{A}_k^{(1)} \otimes \cdots \otimes \mathbf{A}_k^{(n-1)\mathrm{T}}\mathbf{A}_k^{(n-1)}),$$

where the denominator in Eq. (7) is a simplified form. On account of the computer cost, the deduction process can be described as follows:

$$\begin{aligned}
&\left(\mathbf{A}_k^{(N)} \otimes \cdots \otimes \mathbf{A}_k^{(1)}\right)^{\mathrm{T}} \left(\mathbf{A}_k^{(N)} \otimes \cdots \otimes \mathbf{A}_k^{(1)}\right) \mathbf{G}_k^{(n)} \\
&= \left(\mathbf{A}_k^{(1)\mathrm{T}} \otimes \cdots \otimes \mathbf{A}_k^{(N)\mathrm{T}}\right) \left(\mathbf{A}_k^{(N)} \otimes \cdots \otimes \mathbf{A}_k^{(1)}\right) \mathbf{G}_k^{(n)} \\
&= \mathbf{A}_k^{(n)\mathrm{T}}\mathbf{A}_k^{(n)}\mathbf{G}_k^{(n)} \left(\mathbf{A}_k^{(n+1)\mathrm{T}} \otimes \cdots \otimes \mathbf{A}_k^{(N)\mathrm{T}} \otimes \mathbf{A}_k^{(1)\mathrm{T}} \otimes \cdots \otimes \mathbf{A}_k^{(n-1)\mathrm{T}}\right) \\
&\quad \cdot \left(\mathbf{A}_k^{(n+1)} \otimes \cdots \otimes \mathbf{A}_k^{(N)} \otimes \mathbf{A}_k^{(1)} \otimes \cdots \otimes \mathbf{A}_k^{(n-1)}\right) \\
&= \mathbf{A}_k^{(n)\mathrm{T}}\mathbf{A}_k^{(n)} \left(\mathbf{G}_k^{(n)}(\mathbf{A}_k^{(n+1)\mathrm{T}}\mathbf{A}_k^{(n+1)} \otimes \cdots \otimes \mathbf{A}_k^{(N)\mathrm{T}}\mathbf{A}_k^{(N)} \otimes \mathbf{A}_k^{(1)\mathrm{T}}\mathbf{A}_k^{(1)} \otimes \cdots \otimes \mathbf{A}_k^{(n-1)\mathrm{T}}\mathbf{A}_k^{(n-1)})\right).
\end{aligned} \tag{8}$$

Obviously, Eq. (7) follows if the deduction above meets.

When all the mode matrices are fixed, the core tensor could be updated through Eq. (4) and Eq. (6) with the current results, that is

$$\mathcal{G}_k \xleftarrow{fold-n} \mathbf{G}_k^{(n)} \leftarrow \left[\mathbf{A}_k^{(n)}\mathbf{Y}_k^{(n)}\left(\{\mathbf{A}_k^{\otimes -n}\}^{\mathrm{T}}\right)^{\dagger}\right]_+, \tag{9}$$

where the symbol † at the upper right corner returns a Moore-Penrose value within the round bracket, $[\cdot]_+$ denotes the nonnegative constraint on the matrix in the square bracket, which is used to improve the sparseness of the factors for the features (Wang *et al.*, 2016). Actually, with ALS method between $\mathcal{G}_k$ and $\{\mathbf{A}_k^{(n)}|n = 1, 2, 3, \cdots, N\}$, Tucker3 decomposition is realised (Patterson, Gillette, 1977).

If vehicle pass-by noise has K-different features, that is, the tensor is composed by K subtensors, the function can be described as

$$\mathcal{Y} = \sum_{k=1}^{K} \mathcal{Y}_k, \tag{10}$$

where Eq. (10) meets $K \leq N$, $\mathcal{Y}$ is a real value that equals to the noise signal.

2.3. Fast updating algorithm

Updating factors in the process of iterative calculation is beneficial to the efficiency and accuracy (Wang *et al.*, 2013b). However, the factors in a large-span space possibly lead to the problem of mutual interference, due to the reason of nonorthogonal vectors with 3D Cartesian product. For example, we unfold three

different tensors to be matrix form included in three subspaces, respectively, that is:

$$\begin{aligned}\mathbf{U} &= \text{span}\{\mathbf{A}\} = \{\mathbf{a}_k^{(:,1)}, \mathbf{a}_k^{(:,2)} \cdots, \mathbf{a}_k^{(:,N)}\} \\ &= \{\mathbf{u}_1, \mathbf{u}_2, \cdots, \mathbf{u}_N\}, \\ \mathbf{V} &= \text{span}\{\text{vec}(\mathcal{G}_k)\} = \text{span}\{\mathbf{G}_k\} \\ &= \{\mathbf{v}_1, \mathbf{v}_2, \cdots, \mathbf{v}_N\}, \\ \mathbf{W} &= \text{span}\{\text{vec}(\mathcal{Y}_k)\} = \text{span}\{\mathbf{Y}_k\} \\ &= \{\mathbf{w}_1, \mathbf{w}_2, \cdots, \mathbf{w}_N\},\end{aligned} \tag{11}$$

where the matrices $\mathbf{U}$, $\mathbf{V}$, and $\mathbf{W}$ are strictly limited in a different subspace, but are not initialised. When updating one factor, the other two factors must be fixed. The iteration goes on when the new tensor approximates to the original tensor. Part updating procedure can be described as follows:

1. $\mathbf{u}_1 \times \mathbf{v}_1 \to \mathbf{w}_1$;
2. $\mathbf{v}_1 \times \mathbf{w}_1 \to \mathbf{u}_2$;
3. $\{\mathbf{u}_1, \mathbf{u}_2\} \times \mathbf{w}_1 \to \mathbf{v}_2, \mathbf{v}_3$;
4. $\{\mathbf{u}_1, \mathbf{u}_2\} \times \{\mathbf{v}_1, \mathbf{v}_2, \mathbf{v}_3\} \to \mathbf{w}_1, \mathbf{w}_2, \mathbf{w}_3, \mathbf{w}_4, \mathbf{w}_5, \mathbf{w}_6$;
5. $\{\mathbf{v}_1, \mathbf{v}_2, \mathbf{v}_3\} \times \{\mathbf{w}_1, \mathbf{w}_2, \mathbf{w}_3, \mathbf{w}_4, \mathbf{w}_5, \mathbf{w}_6\}$ $\to \mathbf{u}_1, \mathbf{u}_2, \mathbf{u}_3, \mathbf{u}_4, \cdots, \mathbf{u}_{18}$;
6. $\{\mathbf{u}_1, \mathbf{u}_2, \mathbf{u}_3, \mathbf{u}_4, \cdots, \mathbf{u}_{18}\} \times \{\mathbf{w}_1, \mathbf{w}_2, \mathbf{w}_3, \mathbf{w}_4, \mathbf{w}_5, \mathbf{w}_6\}$ $\to \mathbf{v}_1, \mathbf{v}_2, \mathbf{v}_3, \cdots, \mathbf{v}_{108}$;

$\vdots$

Theoretically, the way above, which greatly reduces the cost of the computer storage, avoids restarting the vectors which are not involved in the iteration. Meanwhile, the number of vectors involved increases quickly when the procedure goes forward one by one. More important, it is necessary to keep all the vectors orthogonal, so the steps are restrained as follows:

1) Initialise the vectors $\mathbf{v}_1$ and $\mathbf{w}_1$, that is, $\widehat{\mathbf{v}}_1 \leftarrow \frac{\mathbf{v}_1}{\|\mathbf{v}_1\|_{\mathrm{F}}}$, $\widehat{\mathbf{w}}_1 \leftarrow \frac{\mathbf{w}_1}{\|\mathbf{w}_1\|_{\mathrm{F}}}$. Assume the Cartesian product between the original tensor and the core tensor is $\mathcal{Z}$. Then $\mathbf{u}_2$ will be $\mathbf{u}_2 \leftarrow \mathcal{Z} \times \widehat{\mathbf{v}}_1 \times \widehat{\mathbf{w}}_1$. Unitise vector $\mathbf{u}_2$, then $\mathbf{u}_2 = \frac{\mathbf{u}_2}{\|\mathbf{u}_2\|_{\mathrm{F}}}$.
2) Assume $n := n + 1 (n \leq J)$ and $\mathbf{U}_0 = [\varnothing]$, then the set of vector $\mathbf{u}$ is $\mathbf{u} :\leftarrow \mathcal{Z} \times \widehat{\mathbf{v}}_n \times \widehat{\mathbf{w}}_n$ is orthogonalised as $\widehat{\mathbf{u}} := (\mathbf{I} - \mathbf{U}_{n-1}\mathbf{U}_{n-1}^{\mathrm{T}})\mathbf{u}_n$.
3) Compute $\mathbf{U}_n$. Reunitise the new vector $\widehat{\mathbf{u}}_n \leftarrow \frac{\mathbf{u}_n}{\|\mathbf{u}_n\|}$, and the new mode matrix becomes $\mathbf{U}_n = [\mathbf{U}_{n-1}\widehat{\mathbf{u}}_n]$.
4) Compute $\mathbf{V}_n$. Assume $k = 1 : J_2$, thus $\mathbf{v} :\leftarrow \mathcal{Z} \times \widehat{\mathbf{u}}_n^{\mathrm{T}} \times \mathbf{w}^{\mathrm{T}}$; orthogonalise the vector as $\mathbf{v}_n := (\mathbf{I} - \mathbf{V}_{n-1}\mathbf{V}_{n-1}^{\mathrm{T}})\mathbf{v}_n$; then unitise $\widehat{\mathbf{v}}_n \leftarrow \frac{\mathbf{v}_n}{\|\mathbf{v}_n\|_{\mathrm{F}}}$, so that, $\mathbf{V}_n = [\mathbf{V}_{n-1}\widehat{\mathbf{v}}_n]$.
5) Compute $\mathbf{W}_n$. Assume $n = 1 : J_3$, the set of vector $\mathbf{w}$ is $\mathbf{w} :\leftarrow \mathcal{Z} \times \widehat{\mathbf{u}}_n^{\mathrm{T}} \times \mathbf{v}^{\mathrm{T}}$. Orthogonalising the vector $\mathbf{w}_n := (\mathbf{I} - \mathbf{W}_{n-1}\mathbf{W}_{n-1}^{\mathrm{T}})\mathbf{w}_n$ and unitise $\mathbf{w}_n$, that is, $\widehat{\mathbf{w}}_n \leftarrow \frac{\mathbf{w}_n}{\|\mathbf{w}_n\|_{\mathrm{F}}}$, and the mode matrix $\mathbf{W}$ will be $\mathbf{W}_n = [\mathbf{W}_{n-1}\widehat{\mathbf{w}}_n]$.

NTD with fast updating algorithm is signed as NTD_FUP for short. In step 2) above, the orthogonal method mentioned is similar to the way of Gram-Schmidt decomposition is done, which keeps the vectors normalised. All the factors are constrained to be nonnegative when the iteration continues for sparse matrices as well.

3. Problem description of vehicle pass-by noise

The SPL of vehicle pass-by noise mainly lies in the speed of vehicle/engine, which works both at 2G and 3G with WOT. Mostly, multidirectional noise is likely to dramatically increase the SPL, so it is necessary to improve the performance of the parts/components in the exhaust system, especially in the heat shield.

3.1. Performance problem of current heat shield

The heat shield is installed on the exhaust pipe consists of two-layer aluminium alloy, which prevents the heat transfer and noise radiation during the accelerating process. The two pieces of the heat shields are shown as in Fig. 3.

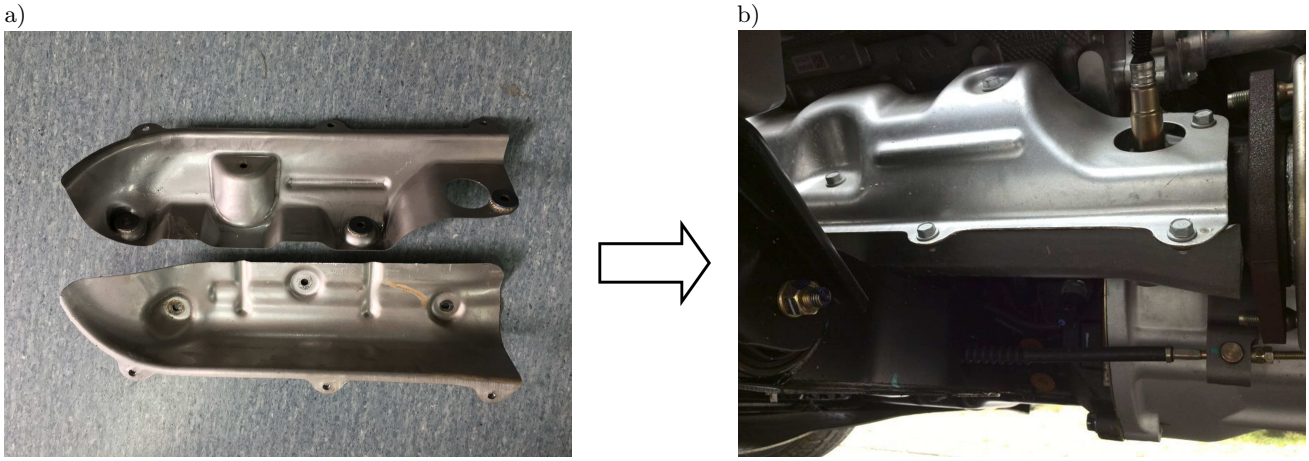

Fig. 3. Installed status of the original heat shield: a) heat shield, b) installed status.

As to the heat shield above, on which the vibration-noise resonance possibly occurs, the frequency of resonant function on the surface of the sheet metal relates to the material itself (Romanowicz, 2014), that is,

$$\omega = \sqrt{\frac{\pi^4 E h^3}{3L^4(1-\mu^2)\rho h}}, \tag{12}$$

where ω is the natural frequency, E is the elastic modulus, h, L are the thickness and the length, respectively, μ is the Poisson ratio, ρ is the density of the heat shield. Then the resonant frequency f_k of the heat shield from Eq. (12) is rewritten as:

$$f_k = \frac{\pi^4 E h^3}{12(1-\mu)L^2}, \tag{13}$$

where the test ground must meet the requirement of the regulation GB 1495–2002 in China (Beijing Labour Protection Research, 2002). The data acquisition system of LMS test.lab is fixed at the position of one of the two microphones. Then the sample frequency as 10240 Hz and the sample time are set to last 10 seconds. The accelerator should be kept on WOT status in the whole process of data acquisition. The data length is chosen as 65536 for bispectrum analysis. With 256 points for each axis, thus, one bispectrum is composed by a matrix with the size 256×256. Two fault statuses are illustrated in Fig. 4 and Fig. 5, where the figures are plotted by the frequency f_1 on x-axis, and the frequency f_2 on y-axis (the same below).

As it can be seen in Fig. 4, the frequency pairs mainly centre around (180, 180) (Hertz, the same below), (100, 180), and (420, 180), (580, 180), where there are too many pairs and it is hard to recognize the frequency of the heat shield. Similarly, the noise of the low frequency happens on 3G in Fig. 5a and Fig. 5b.

The maximum amplitudes of the vibration frequency of the features extracted point to (180, 180), (340, 180), (560, 180) and (740, 180), respectively, and hardly interpret where the fault comes. Mostly, the radiation noise comes in the secondary interference, which amplifies the SPL of the vehicle pass-by noise both in Fig. 4 and Fig. 5, and results in too many frequency pairs to recognise. Therefore, the frequency of the basis images should be improved for sparse and clear bispectrum features.

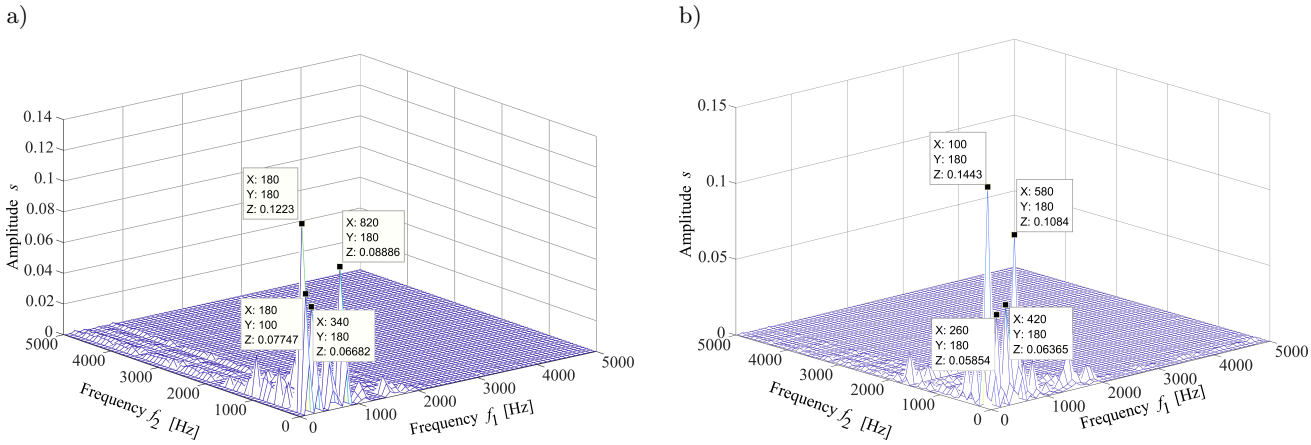

Fig. 4. Part origin basis images of 2G status with main frequency pair: a) (180, 180), b) (100, 180).

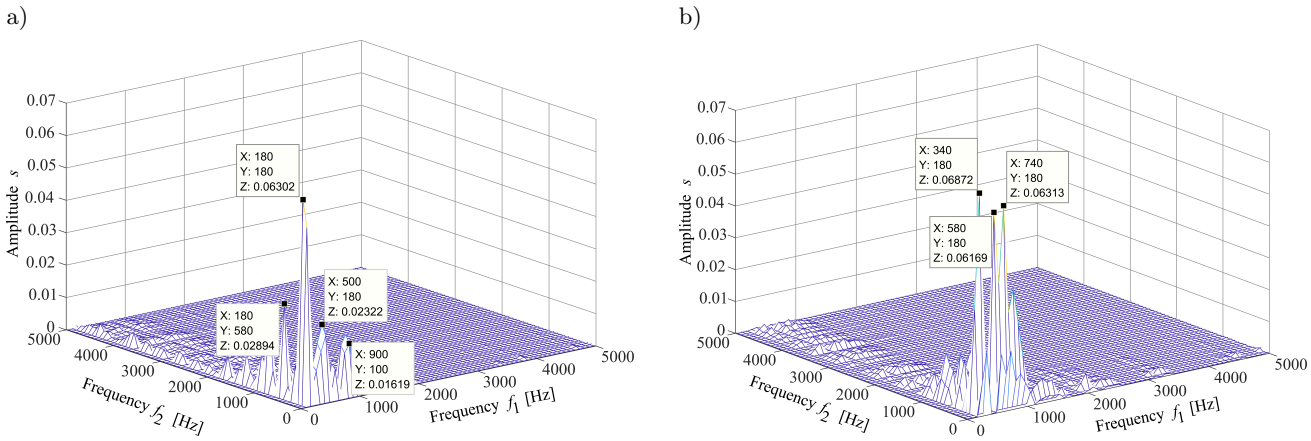

Fig. 5. Part origin basis images of 3G status with main frequency pair: a) (180, 180), b) (180, 340).

3.2. SPL of vehicle pass-by noise with the original heat shield

As one of the most important evaluation indexes to vehicle pass-by noise, the SPL meets most people's psychology characteristics, so the A-weighted SPL based on logarithmic function by Nilsson (2007) is written as:

$$L_p = \log_{10} \frac{P^2}{P_0^2}, \tag{14}$$

where L_p denotes the SPL value, P is the current sound pressure, P_0 is the referenced equivalent threshold of sound pressure, that is, 2×10^{-5} Pa. In GB 1495–2002 (Beijing Labor Protection Research, 2002, p. 2), the average value is included both at the left and the right side tested, and the mean value equals to the larger one between the average values (subtract 1 dB(A) only to K-cars) Then the final evaluation value equals to the average value of mean values of 2G and 3G. The results are listed as in Table 1.

Table 1. SPL of vehicle pass-by noise with the original heat shield.

Gear range	Position	Test number	Test result [dB(A)]	Average value [dB(A)]	Mean value [dB(A)]	Evaluating value [dB(A)]
2G	Left	1	79.2	79.4	78.4	76.2
		2	79.5			
		3	79.4			
		4	79.4			
	Right	1	79.5	79.3		
		2	78.8			
		3	79.5			
		4	79.2			
3G	Left	1	75.9	75.1	74.1	
		2	73.8			
		3	74.6			
		4	75.9			
	Right	1	75.1	74.5		
		2	74.1			
		3	74.6			
		4	74.3			

In Table 1, the evaluating value still exceeds 0.2 dB(A) as compared with the specified SPL of 76 dB(A), according to the GB 1495–2002 which limits the vehicle noise emission on the road. Therefore, some improved measures are necessary to move to lower SPL.

4. Feature extracted by NTD_FUP for bispectrum analysis

4.1. Performance comparison with other traditional methods

In this section, NTD_FUP is compared with other typical algorithms in the performance of tensor decomposition. One of the existing methods is NTF, which is a special form of NTD with diagonal unit values fully in the core tensor and which uses traditional alternative least square (ALS) to calculate the vectors one by one in a factor in the iteration, namely NTF_ALS. NTD with ALS (NTD_ALS), which is similar to NTF_ALS, calculates the vectors one by one. NTD with Hierarchical ALS (NTD_HALS, Cichocki *et al.*, 2009) performs a factor-by-factor procedure instead of updating column-by-column vectors, according to the hierarchy of features. NTD with beta divergences (NTD_Beta, Cichocki, Amari, 2010) belongs to the exponential dispersion model family of distributions, a generalisation of the exponential family, which are the response distributions for generalised linear models. The last one is NTD with alpha divergences (NTD_Alpha, Cichocki, Amari, 2010), whose minimisation of Alpha-divergence is based on the projected quasi-Newton method, whereby the adaptively-regularised Hessian within the Levenberg-Marquardt approach is inverted using the QR decomposition. When the methods are used to decompose the same size tensor, the deviation of successive relative error (DSRE) as an evaluation index is marked as γ, that is,

$$\gamma = -20 \log_{10} \frac{\left\| \widehat{\mathcal{Y}} - \mathcal{Y} \right\|_{\mathrm{F}}}{\mathcal{Y}_{\mathrm{F}}}, \tag{15}$$

where Eq. (15) means the higher DSRE and a higher accuracy, respectively. In the experiment, the DSRE and the computation time are adopted as two evaluation indexes for those methods' comparison. Besides, the rank of the core tensor is also chosen as (128, 128, 32) for the candidate tensors. Results of all methods for DSRE (γ/dB) and time (t/s) are recorded in Table 2.

In order to observe the results intuitively, the bar diagrams have been generated from Table 2 and are shown in Fig. 6.

As it can be seen in the bar diagram above, combining with the results recorded, it is easy to find that the maximum DESR arrives at 50.16 dB by NTD_FUP against other methods under the same condition. According to Eq. (15), NTD_FUP performs less computation error compared with other methods listed. Particularly, the NTF_ALS algorithm takes more than 3100.0 s to decompose the tensor with the size $256 \times 256 \times 64$ in Fig. 6b, it only gets the DSRE at 20.31 dB. The NTD_ALS takes less time than

Table 2. Computation results of different methods from three dataset.

Method	$256 \times 256 \times 40$		$256 \times 256 \times 48$		$256 \times 256 \times 64$	
	DSRE [dB]	Time [s]	DSRE [dB]	Time [s]	DSRE [dB]	Time [s]
NTF_ALS	18.32	1625.7	19.24	2169.6	20.31	3109.0
NTD_ALS	22.14	1054.0	22.25	1325.5	23.57	1817.6
NTD_HALS	31.59	1531.0	31.36	1687.5	32.22	1865.6
NTD_Alpha	36.65	1836.2	38.15	2164.6	39.68	2304.9
NTD_Beta	40.61	1706.4	39.46	1968.3	39.87	2465.6
NTD_FUP	48.10	1687.5	50.24	1762.3	50.16	1905.4

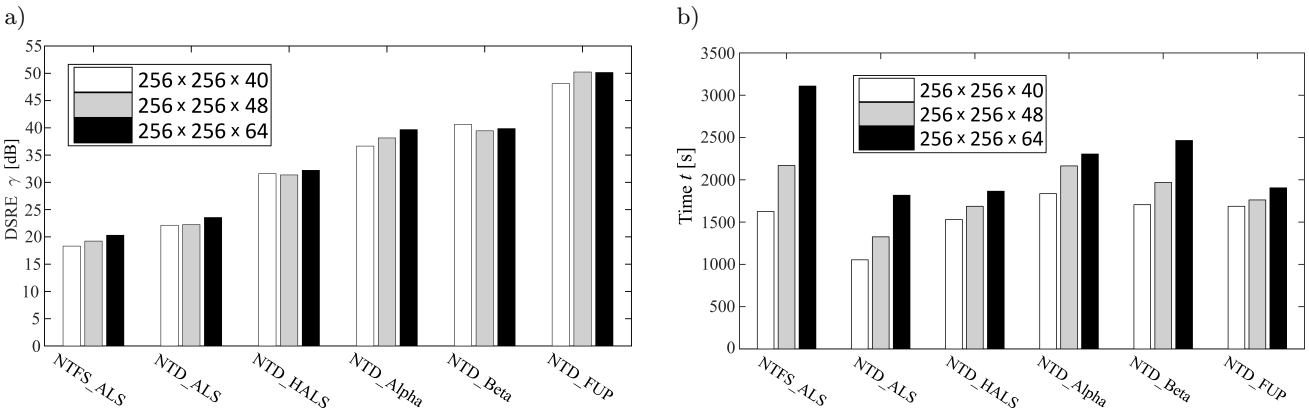

Fig. 6. Bar comparison of different methods: a) computation accuracy, b) computation time.

NTD_FUP, according to Table 2. However, the updating procedure is not implemented due to the algorithm limitation itself, which results in a bigger error under the same condition. Generally, the updating algorithms implemented in NTD_HALS, NTD_Alpha, NTD_Beta, NTD_FUP have comparatively fewer errors than NTF_ALS and NTD_ALS, which calculate the factors without updating. This is especially clear from the last row of Table 2, the larger tensor, the less time is used by NTD_FUP. Therefore, NTD_FUP is superior to traditional methods both in accuracy and time in the case of large tensors.

4.2. Bispectrum analysis from the basis features extracted by NTD_FUP

With the data collected before, the tensor about vehicle pass-by noise is composed by the slice matrices, which adds 0.1:0.01:6.4 dB white noise. Thus, the size of the reconstructed tensor is $256 \times 256 \times 64$. Set the dimensions (128, 128, 32) as the rank of the core tensor (Wang *et al.*, 2013b). Then partial basis images of bispectrum features are extracted by NTD_FUP on 2G at WOT shown in Fig. 7.

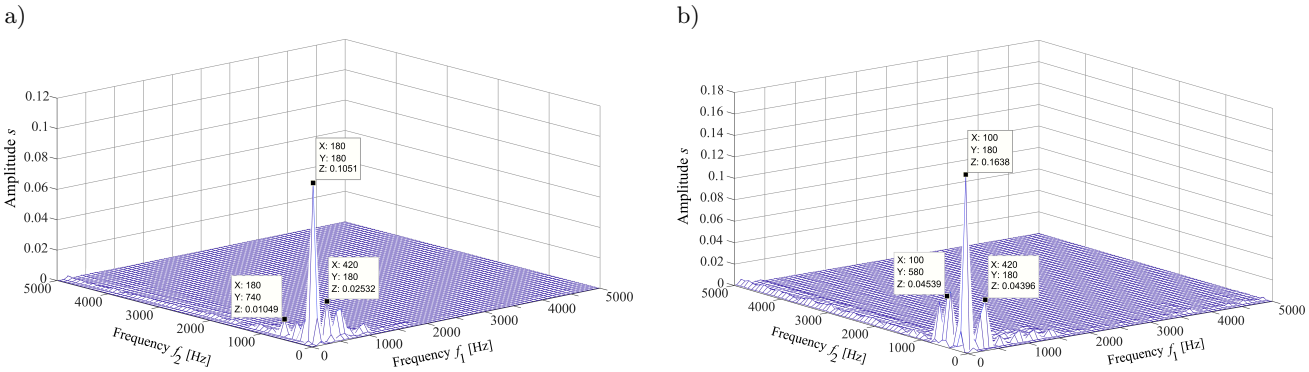

Fig. 7. Partially improved basis images of 2G status with main frequency pair: a) (180, 180), b) (100, 180).

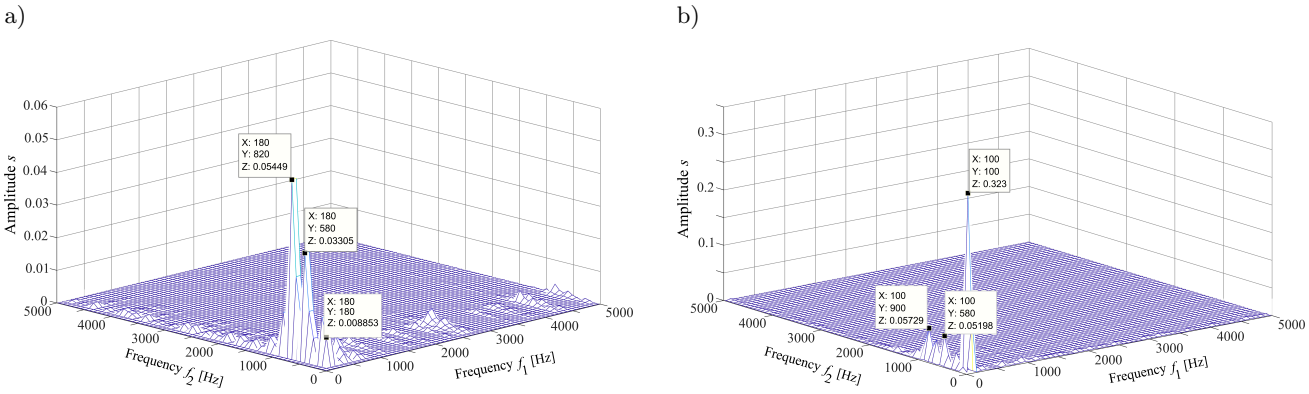

Fig. 8. Partial basis images of 3G status with main frequency pair: a) (180, 180), b) (100, 100).

As the basis images in Fig. 7 above show, the sparseness of the bispectrum features is improved compared with Fig. 4 and Fig. 5. The dominant frequency pairs of the features centre around (180, 180) and (100, 180), which meets the frequency in Fig. 4, and help to find the main parts/components in the exhaust system. Similarly, partial basis images on 3G status are shown in Fig. 8.

In Fig. 8a, the reduced amplitude of the bispectrum of frequency pair approximate to (180, 180), while the dominant frequency pairs range from (100, 180) to (100, 100) in Fig. 8b, which exposes the frequency of semi-order noise of the heat shield, possibly masked in Fig. 5. So these features provide engineers with more information for fault interpretation, which is crucial for the design of the parts/components for the SPL reduction of vehicle pass-by noise.

4.3. Improved heat shield

The material selection plays an important part in voiding the noise radiation, which involves the design of the central frequency f_c in Eq. (1). Synthetically, the aluminum-foil alloy is considered as the material of the heat shield, according to the property of well thermal conductivity and low density itself. Two sample pieces of heat shield with the same size are illustrated in Fig. 9.

As shown in Fig. 9, the improved heat shields consist of two-tier aluminum-foil with many uniform pits on it with the size of $10 \times 10 \times 2$ mm (length $\times$ wide $\times$ depth), which helps to avoid the vibration-noise working at the same direction on the surface of the heat shield. Thus, the input in different directions lowers the possibility of the vibration-noise resonance . What is more, the light and soft alloy helps to lower the stiffness of the heat shield, which cuts down the sharpness of the noise for sound quality (Wang *et al.*, 2016). The SPL of the vehicle pass-by noise as the evaluating value is recorded in Table 3.

In Table 3, the evaluating value marked 75.3 dB(A), which meets the requirement of SPL 76 dB(A) in the regulation, is 0.9 dB(A) lower than the one in Table 1 by the improved heat shield. Apparently, the SPLs both on the left and the right have been reduced. The comparison between the original and the improved heat shields is shown in Fig. 10.

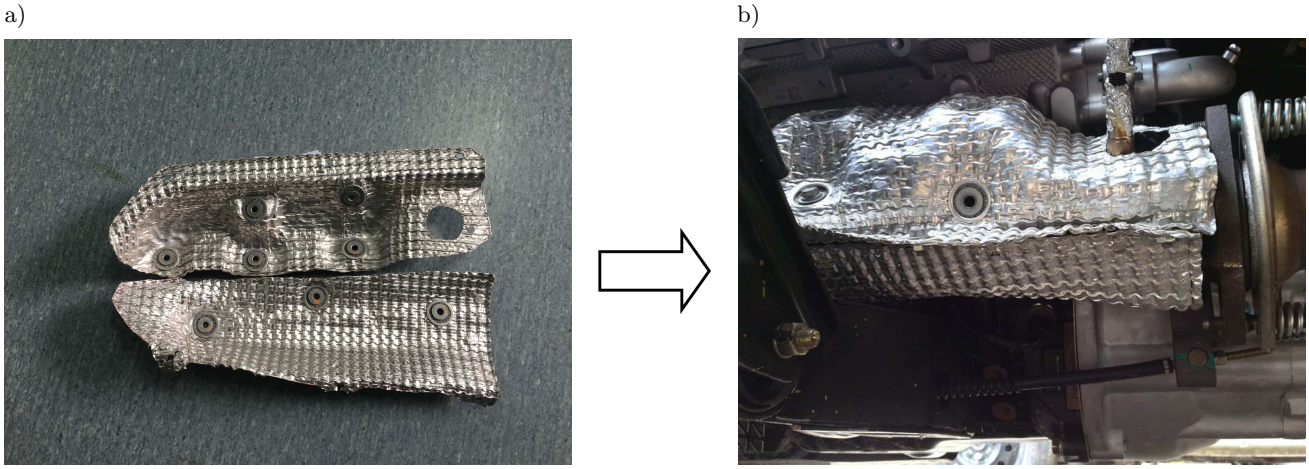

Fig. 9. Installation status of the improved heat shield: a) the improved heat shield, b) installation on the heat shield.

Table 3. SPL of vehicle pass-by noise with the improved heat shield.

Gear range	Position	Test number	Test result [dB(A)]	Average value [dB(A)]	Mean value [dB(A)]	Evaluating value [dB(A)]
2G	Left	1	77.5	77.3	76.8	75.3
		2	77.3			
		3	76.9			
		4	77.3			
	Right	1	77.6	77.8		
		2	78.1			
		3	77.9			
		4	77.6			
3G	Left	1	74.9	74.4	73.7	
		2	73.7			
		3	74.0			
		4	74.9			
	Right	1	75.1	74.7		
		2	74.3			
		3	74.6			
		4	74.8			

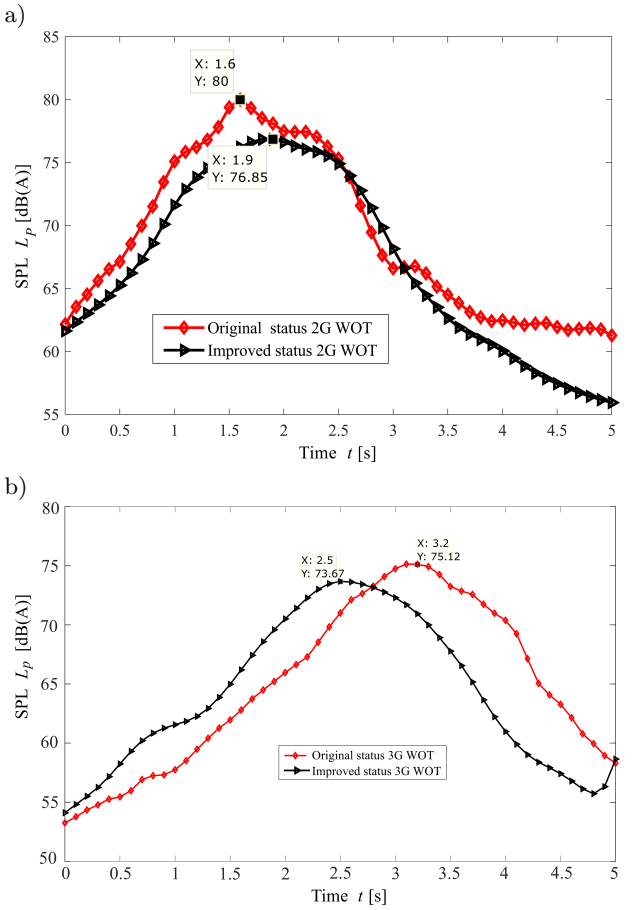

Fig. 10. SPL comparison of vehicle pass-by noise between 2G and 3G: a) SPL at the WOT status of 2G, b) SPL at the WOT status of 3G.

In Fig. 10, the maximum SPL both at 2G and 3G is lower than the ones with the original heat shield under the same conditions. The SPL has been reduced by 1.45 dB(A) at 3G status. Particularly, a reduction of near 3.2 dB(A) of SPL at 2G status is achieved, compared with the maximum value when the heat shields are not improved. This result demonstrates that the SPL now meets the limitation requirement of the regulation.

4.4. Results and discussion

Many useful features of vehicle pass-by noise are interfered with irrelevant signals. The frequency pairs such as (180, 100), (250, 180), (500, 180), (340, 180) in Fig. 4 and Fig. 5, allow us to know that the dominant frequency of parts/components should be improved in application. Such difficulties still exist because the unsparseness features dramatically affect the judgement of the fault statuses. NTD_FUP is used to extract the bispectrum with the feature based on its performances of computation time and sparser features, which is able to correctly interpret the fault present in the parts/components. However, it fails to find out one special part/component depending on the bispectrum alone, especially for an engineer in the case of not understanding the structure of the exhaust system. So how to explore the phase angle of bispectum features to provide with exact information is a significant challenge for solving the NVH problem.

NTD_FUP is successfully used to bispectrum analysis for part design of exhaust systems. The knowledge of NTD is very important to promote the new technology applied into fault diagnosis of an automobile.

5. Conclusions

1) NTD_FUP method has comprehensively superior performances both in computation accuracy and time compared with other traditional methods.
2) NTD_FUP method is successfully applied into extracting the bispectrum features, which determines the natural frequency of the parts/components in the exhaust system.
3) The material of aluminum-foil alloy replaces the aluminum alloy alone. The new material improves the performance of the heat shield such as light design and low noise radiation.
4) The SPL of vehicle pass-by noise has been lowered by 0.9 dB(A) by using the improved heat shield under the same condition.

Acknowledgment

This project is supported by the fund project of SAIC-GM-Wuling Automobile CO., LTD (Grant

No. N300-N12, No. CN201S-B15T, No. CN180). The authors are thankful to all the engineers of the project who gave their strong support as well.

References

1. Andersson C.A., Bro R. (1998), *Improving the speed of multi-way algorithms: Part I. Tucker3*, Chemometrics and Intelligent Laboratory Systems, **42**, 93–103, http://dx.doi.org/10.1016/S0169-7439(98)00010-0.

2. Bader B.W, Kolda T.G. (2006), *Algorithm 862: MATLAB tensor classes for fast algorithm prototyping*, ACM Transactions on Mathematical Software, **32**, 635–653, http://dx.doi.org/10.1145/1186785.1186794.

3. Braun M.E., Walsh S.J., Horner J.L., Chuter R. (2013), *Noise source characteristics in the ISO 362 vehicle pass-by noise test: Literature review*, Applied Acoustics, **74**, 1241–1265, http://dx.doi.org/doi:10.1016/j.apacoust.2013.04.005.

4. Buciu I., Pitas I. (2006), *NMF, LNMF, and DNMF modeling of neural receptive fields involved in human facial expression perception*, Journal of Visual Communication and Image Representation, **17**, 958–969, http://dx.doi.org/10.1016/j.jvcir.2006.06.001.

5. Beijing Labor Protection Research (2002), *Limits and measurement methods for noise emitted by accelerating motor vehicles* [in Chinese], GB 1495–2002, http://www.pv265.com/gjbz/201112/7319.html.

6. Cichocki A., Amari S. (2010), *Families of Alpha-Beta- and Gamma- Divergences: Flexible and Robust Measures of Similarities*, Entropy, **12**, 1532–1568, http://dx.doi.org/10.3390/e12061532.

7. Cichocki A., Zdunek R., Phan A.H., Amari S.I. (2009), *Nonnegative matrix and tensor factorizations: Applications to exploratory multi-way data analysis and blind source separation*, John Wiley & Sons, http://dx.doi.org/10.1002/9780470747278.

8. Davies P., Harrison M. (1997), *Predictive acoustic modelling applied to the control of intake/exhaust noise of internal combustion engines*, Journal of Sound and Vibration, **202**, 249–274, http://dx.doi.org/10.1006/jsvi.1996.0842.

9. Hemmateenejad B., Javidnia K., Saeidi-Boroujeni M. (2008), *Spectrophotometric monitoring of nimesulide photodegradation by a combined hard-soft multivariate curve resolution-alternative least square method*, Journal of Pharmaceutical and Biomedical Analysis, **47**, 3, 625–630, http://dx.doi.org/10.1016/j.jpba.2008.01.040.

10. Kim Y.D., Choi S.J. (2007), *Nonnegative tucker decomposition*, 2007 IEEE Conference on Computer Vision and Pattern Recognition, **1–8**, pp. 3104–3111, Minneapolis, MN, http://dx.doi.org/10.1109/CVPR.2007.383405.

11. Kopriva I., Cichocki A. (2010), *Nonlinear band expansion and 3D nonnegative tensor factorization for blind decomposition of magnetic resonance image of the brain*, International Conference on Latent Variable Analysis and Signal Separation, **6363**, pp. 490–497, St. Malo, France, http://dx.doi.org/10.1007/978-3-642-15995-4_61.

12. Lim L.H., Comon P. (2010), *Multiarray signal processing: Tensor decomposition meets compressed sensing*, Comptes Rendus Mecanique, **338**, 6, 311–320, http://dx.doi.org/10.1016/j.crme.2010.06.005.

13. Mongia R.K., Bhartia P. (1994), *Dielectric resonator antennas. A review and general design relations for resonant frequency and bandwidth*, International Journal of Microwave and Millimeter-Wave Computer Aided Engineering, **4**, 230–247, http://onlinelibrary.wiley.com/doi/10.1002/mmce.4570040304/pdf.

14. Nilsson M.E. (2007), *A-weighted sound pressure level as an indicator of short-term loudness or annoyance of road-traffic sound*, Journal of Sound and Vibration, **302**, 197–207, http://dx.doi.org/10.1016/j.jsv.2006.11.010.

15. Okokon E.O., Turunen A.W., Ung-Lanki S., Vartiainen A.K., Tiittanen P., Lanki T. (2015), *Road-traffic noise: annoyance, risk perception, and noise sensitivity in the finnish adult population*, International Journal of Environmental Research and Public Health, **12**, 5712–5734, http://dx.doi.org/10.3390/ijerph120605712.

16. Park S.H., Kim Y.H. (2001), *Visualization of pass-by noise by means of moving frame acoustic holography*, Journal of the Acoustical Society of America, **110**, 2326–2339, http://dx.doi.org/10.1121/1.1404976.

17. Patterson E., Gillette D. (1977), *Commonalities in measured size distributions for aerosols having a soil – derived component*, Journal of Geophysical Research, **82**, 2074–2082, http://dx.doi.org/10.1029/JC082i015p02074.

18. Romanowicz B. (2014), *Surface Waves*, Encyclopedia of Solid Earth Geophysics, Springer Netherlands, pp. 1406–1419, http://dx.doi.org/10.1007/978-90-481-8702-7_143.

19. Xu Y.Y., Yin W.T. (2013), *A block coordinate descent method for regularized multiconvex optimization with applications to nonnegative tensor factorization and completion*, SIAM Journal on Imaging Sciences, **6**, 1758–1789, http://dx.doi.org/10.1137/120887795.

20. Wang C., He X., Bu J., Chen Z., Chen C., Guan Z. (2011), *Image representation using Laplacian regularized nonnegative tensor factorization*, Pattern Recognition, **44**, 2516–2526, http://dx.doi.org/10.1016/j.patcog.2011.03.021.

21. Wang H., Xu F., Jia M., Hu J., Huang P. (2013a), *Research on exponential regularization approach for*

nonnegative Tucker3 decomposition, Optik – International Journal for Light and Electron Optics, **124**, 6615–6621, http://dx.doi.org/10.1016/j.ijleo. 2013.05. 024.

22. Wang H.J., Deng G.Y., Li Q.L., Kang Q. (2016), *Research on bispectrum analysis of secondary feature for external vehicle noise based on nonnegative tucker3 decomposition*, Eksploatacja i Niezawodność – Maintenance and Reliability, **18**, 291–298, http://dx.doi.org/10.17531/ein.2016.2.18.

23. Wang H.J., Xu F.Y., Zhao J., Jia M.P., Hu J.Z., Huang P. (2013b), *Bispectrum feature extraction of gearbox faults based on nonnegative Tucker3 decomposition with 3D calculations*, Chinese Journal of Mechanical Engineering, **26**, 1182–1193, http://dx.doi.org/10.3901/CJME.2013.06.1182.